Author/s:
Holliday, H;Yang, J;Dodson, E;Nikolic, I;Kamili, A;Wheatley, M;Deng, N;Alexandrou, S;Davis, TP;Kavallaris, M;Caldon, CE;McCarroll, J;De Preter, K;Mestdagh, P;Marshall, GM;Simpson, KJ;Fletcher, J;Swarbrick, A

Title:
miR-99b-5p, miR-380-3p, and miR-485-3p are novel chemosensitizing miRNAs in high-risk neuroblastoma

Date:
2022-03-02

Citation:
Holliday, H., Yang, J., Dodson, E., Nikolic, I., Kamili, A., Wheatley, M., Deng, N., Alexandrou, S., Davis, T. P., Kavallaris, M., Caldon, C. E., McCarroll, J., De Preter, K., Mestdagh, P., Marshall, G. M., Simpson, K. J., Fletcher, J. & Swarbrick, A. (2022). miR-99b-5p, miR-380-3p, and miR-485-3p are novel chemosensitizing miRNAs in high-risk neuroblastoma. Molecular Therapy, 30 (3), pp.1119-1134. https://doi.org/10.1016/j.ymthe.2022.01.004.

Persistent Link:
https://hdl.handle.net/11343/335521

Molecular Therapy
Original Article

miR-99b-5p, miR-380-3p, and miR-485-3p are novel chemosensitizing miRNAs in high-risk neuroblastoma

Holly Holliday,[1,2,3,4] Jessica Yang,[1,12] Eoin Dodson,[1,12] Iva Nikolic,[5,6] Alvin Kamili,[3,4] Madeleine Wheatley,[3] Niantao Deng,[1,2] Sarah Alexandrou,[1,2] Thomas P. Davis,[7,8] Maria Kavallaris,[3,4,9] C. Elizabeth Caldon,[1,2] Joshua McCarroll,[3,4,9] Katleen De Preter,[10] Pieter Mestdagh,[10] Glenn M. Marshall,[3,11] Kaylene J. Simpson,[5,6] Jamie Fletcher,[3,4] and Alexander Swarbrick[1,2]

[1]Garvan Institute of Medical Research, Darlinghurst, NSW 2010, Australia; [2]St Vincent's Clinical School, Faculty of Medicine, UNSW Sydney, Sydney, NSW 2010, Australia; [3]Children's Cancer Institute, Lowy Cancer Research Centre, UNSW Sydney, Sydney, NSW 2031, Australia; [4]School of Women's and Children's Health, UNSW Sydney, Sydney, NSW 2052, Australia; [5]Victorian Centre for Functional Genomics, Peter MacCallum Cancer Centre, Melbourne, VIC 3002, Australia; [6]Sir Peter MacCallum Department of Oncology, University of Melbourne, Melbourne, VIC 3002, Australia; [7]ARC Centre of Excellence in Convergent Bio-Nano Science & Technology, Australian Institute for Bioengineering, The University of Queensland, Brisbane, QLD 2072, Australia; [8]ARC Centre of Excellence in Convergent Bio-Nano Science & Technology, Monash Institute of Pharmaceutical Sciences, Monash University, Melbourne, VIC 3052, Australia; [9]Australian Centre for Nanomedicine, UNSW Sydney, Sydney, NSW 2052, Australia; [10]Cancer Research Institute Ghent, Ghent University, Ghent B-9000, Belgium; [11]Kids Cancer Centre, Sydney Children's Hospital, Sydney, NSW 2031, Australia

Neuroblastoma is a deadly childhood cancer arising in the developing sympathetic nervous system. High-risk patients are currently treated with intensive chemotherapy, which is curative in only 50% of children and leaves some surviving patients with life-long side effects. microRNAs (miRNAs) are critical regulators of neural crest development and are deregulated during neuroblastoma tumorigenesis, making miRNA-based drugs an attractive therapeutic avenue. A functional screen of >1,200 miRNA mimics was conducted in neuroblastoma cell lines to discover miRNAs that sensitized cells to low doses (30% inhibitory concentration [IC_{30}]) of doxorubicin and vincristine chemotherapy used in the treatment of the disease. Three miRNAs, miR-99b-5p, miR-380-3p, and miR-485-3p, had potent chemosensitizing activity with doxorubicin in multiple models of high-risk neuroblastoma. These miRNAs underwent genomic loss in a subset of neuroblastoma patients, and low expression predicted poor survival outcome. *In vitro* functional assays revealed each of these miRNAs enhanced the anti-proliferative and pro-apoptotic effects of doxorubicin. We used RNA sequencing (RNA-seq) to show that miR-99b-5p represses neuroblastoma dependency genes *LIN28B* and *PHOX2B* both *in vitro* and in patient-derived xenograft (PDX) tumors. Luciferase reporter assays demonstrate that *PHOX2B* is a direct target of miR-99b-5p. We anticipate that restoring the function of the tumor-suppressive miRNAs discovered here may be a valuable therapeutic strategy for the treatment of neuroblastoma patients.

INTRODUCTION

Neuroblastoma is a childhood cancer that arises in the developing sympathetic nervous system, giving rise to tumors in the adrenal glands and sympathetic ganglia.[1] Ninety percent of cases are diagnosed in young children under the age of 10, with a median age of diagnosis at 18 months.[1] Like other pediatric cancers, neuroblastoma has a low mutational burden and is instead characterized by whole chromosome or large segmental DNA copy-number alterations and epigenetic rewiring.[1,2] Amplification of MYCN occurs in 20%–25% of cases and is used as a biomarker for the high risk of relapse and chemoresistance.[3,4] Despite intensive multimodal therapy, which involves high-dose chemotherapy, radiotherapy, and immunotherapy, the 5-year survival rate for high-risk patients is below 50%, and surviving patients suffer from chronic treatment-related morbidity.[5–9] New therapies that can either replace or significantly improve the current therapy are urgently needed.

MicroRNAs (miRNAs) are small non-coding RNAs that bind through imperfect complementarity to the 3′ UTR of mRNA transcripts to silence gene expression by causing mRNA destabilization or repression of translation.[10] Up to 60% of human protein-coding genes are estimated to be regulated by miRNAs, and a single miRNA can regulate hundreds of different transcripts.[11,12] miRNAs regulate a myriad of cellular processes from proliferation and differentiation to apoptosis, making these regulators essential for normal development. Deregulation of miRNA expression through genomic events, such as mutations, deletions and amplifications, or alterations in miRNA

Received 1 June 2021; accepted 3 January 2022;
https://doi.org/10.1016/j.ymthe.2022.01.004.

[12]These authors contributed equally

Correspondence: Alexander Swarbrick, Garvan Institute of Medical Research, Darlinghurst, NSW 2010, Australia.
E-mail: a.swarbrick@garvan.org.au

biogenesis enzymes, contributes to human disease etiology such as cancer.[13,14]

Insights into miRNA biology in cancer have made miRNAs attractive tools and targets for novel therapeutic approaches.[14] Administering synthetically derived miRNA mimics that replenish the activity of mutated or deleted tumor-suppressive miRNAs or the inhibition of endogenous oncogenic miRNAs are two strategies for miRNA-based cancer therapeutics. The relatively convenient synthesis of miRNA-based therapies makes them particularly desirable, potentially bypassing years of costly medicinal chemistry associated with the development of other drugs such as small-molecule inhibitors.

miRNA expression is globally reduced in cancer cells compared with in normal cells,[15] arguing that this provides an advantage for tumorigenesis and/or treatment resistance. A significant challenge in developing miRNA therapeutics is the identification of the most suitable miRNA candidates for each cancer type. Several miRNAs have been implicated in neuroblastoma tumorigenesis such as miR-34a,[16] miR-380-5p,[17] miR-17-92,[18] let-7,[19] and miR-204.[20] Further to these reports, we recently used an unbiased screening approach to identify other miRNAs that were lethal to neuroblastoma cells and mapped these to their targets.[21]

We hypothesize that the loss of miRNA expression is not only tumorigenic but can also promote drug resistance. The majority of high-risk neuroblastoma patients receive systemic chemotherapy; therefore, we conducted a screen to specifically find miRNAs that could sensitize cells to chemotherapy. Combination therapy is more likely to lead to sustained cancer control, and new therapeutics are generally first combined with standard-of-care therapies in clinical trials. Furthermore, therapies that specifically sensitize cancer cells to chemotherapy are less likely to be toxic to normal cells. Here, we report the results of an unbiased functional screen in neuroblastoma-identifying miRNAs that sensitized neuroblastoma cells to low-dose chemotherapy. Three candidate miRNAs were followed up with for further study: miR-99b-5p, miR-380-3p, and miR-485-3p. The antiproliferative and pro-apoptotic functions of these miRNAs were experimentally validated in multiple models. Furthermore, we used transcriptomics to show that miR-99b-5p targets key neuroblastoma essentiality genes *PHOX2B* and *LIN28B*. These findings are an initial step toward therapies that spare patients from high doses of chemotherapy and the resulting toxic side effects.

RESULTS

High-throughput functional screening identifies chemosensitizing miRNAs in MYCN-amplified neuroblastoma cells

To discover miRNAs with therapeutic potential, we performed a high-throughput miRNA screen as outlined in Figure 1A. The screen was performed in two neuroblastoma cell lines: MYCN-amplified Kelly cells and non-MYCN-amplified SH-EP cells. Cells were transfected with a library of 1,240 individual miRNA mimics and were then treated with two standard-of-care chemotherapeutic agents with distinct mechanisms, the anthracycline drug doxorubicin and the vinca alkaloid drug vincristine (Table S1). Cells were treated with 30% inhibitory concentration (IC_{30}) doses of chemotherapy in order to identify miRNAs that sensitize the cells to low doses of chemotherapy. The screen identified two classes of putative therapeutic miRNAs: chemosensitizing hits, which had a minimal effect in the vehicle-treated cells but cooperated with chemotherapy to kill the cells (>65% viability in vehicle and <50% viability in chemotherapy-treated cells), and lethal hits, which killed cells regardless of whether chemotherapy was present or absent (viability <50% in both vehicle- and chemotherapy-treated cells). We previously described the lethal miRNA hits[21] and focused exclusively on the chemosensitizing mimics in the present study. More chemosensitizing hits were observed in the MYCN-amplified Kelly cell line (107 mimics across both drugs) than in the non-MYCN-amplified SH-EP cell line (10 mimics) (Figures 1B and S1A). The doxorubicin-sensitizing miRNAs appeared to have a more pronounced effect on viability than did the vincristine-sensitizing miRNAs in Kelly cells, when combined with the respective chemotherapeutic agent (Figure 1B).

To test the reproducibility of the screen, we performed a secondary screen with a subset of 48 miRNAs in Kelly cells and an additional MYCN-amplified cell line, SK-N-DZ. Twenty-two chemosensitizing, 11 lethal, and 15 non-active mimics were included for validation. We observed a strong Peason correlation (R^2 = 0.86) between the two screens in Kelly cells (Figure S1B). Out of the 22 tested chemosensitizing mimics, 10 were validated in Kelly cells (miR-100-5p, miR-99b-5p, miR-380-3p, miR-515-3p, miR-3924, miR-485-3p, miR-3646, miR-449a, miR-34a-5p, and miR-34c-5p) and 6 of these validated in SK-N-DZ cells (miR-100-5p, miR-99b-5p, miR-380-3p, miR-515-3p, miR-3924, and miR-449a) (Figure 1C). Validated chemosensitizing hits included well-known tumor-suppressive miRNAs such as miR-34a-5p and miR-34c-5p.[22,23]

To further narrow down the validated chemosensitizing mimics, we excluded miR-34c-5p and miR-449a, as these miRNAs were previously reported to be toxic to cardiomyocytes.[24] The viability of neuroblastoma cells transfected with mimics of the remaining 5 candidate miRNAs (miR-99b-5p, miR-380-3p, miR-485-3p, miR-515-3p, and miR-34a-5p) in neuroblastoma cells lines are visualized as bar graphs in Figure 1D. The chemosensitization of these miRNAs was specific to MYCN-amplified Kelly and SK-N-DZ cells and was not observed in the MYCN-non-amplified SH-EP cell line. Finally, we tested the mimics for toxicity in an immortalized fibroblast cell line, IMR-90 (Figure 1D), and the normal breast epithelial cell line MCF10A[21] (Figure S1C). This eliminated miR-515-3p and miR-34a-5p, as they killed at least 50% of normal cells in the absence of chemotherapy. This left 3 candidate miRNAs, miR-99b-5p, miR-380-3p, and miR-485-3p, that specifically sensitized MYCN-amplified neuroblastoma cells to doxorubicin with minimal toxicity or chemosensitizing activity in normal cells.

Candidate miRNAs are putative tumor suppressors in neuroblastoma patients

To determine if expression of the candidate miRNAs is associated with clinical parameters, we analyzed a cohort of 255 primary neuroblastoma

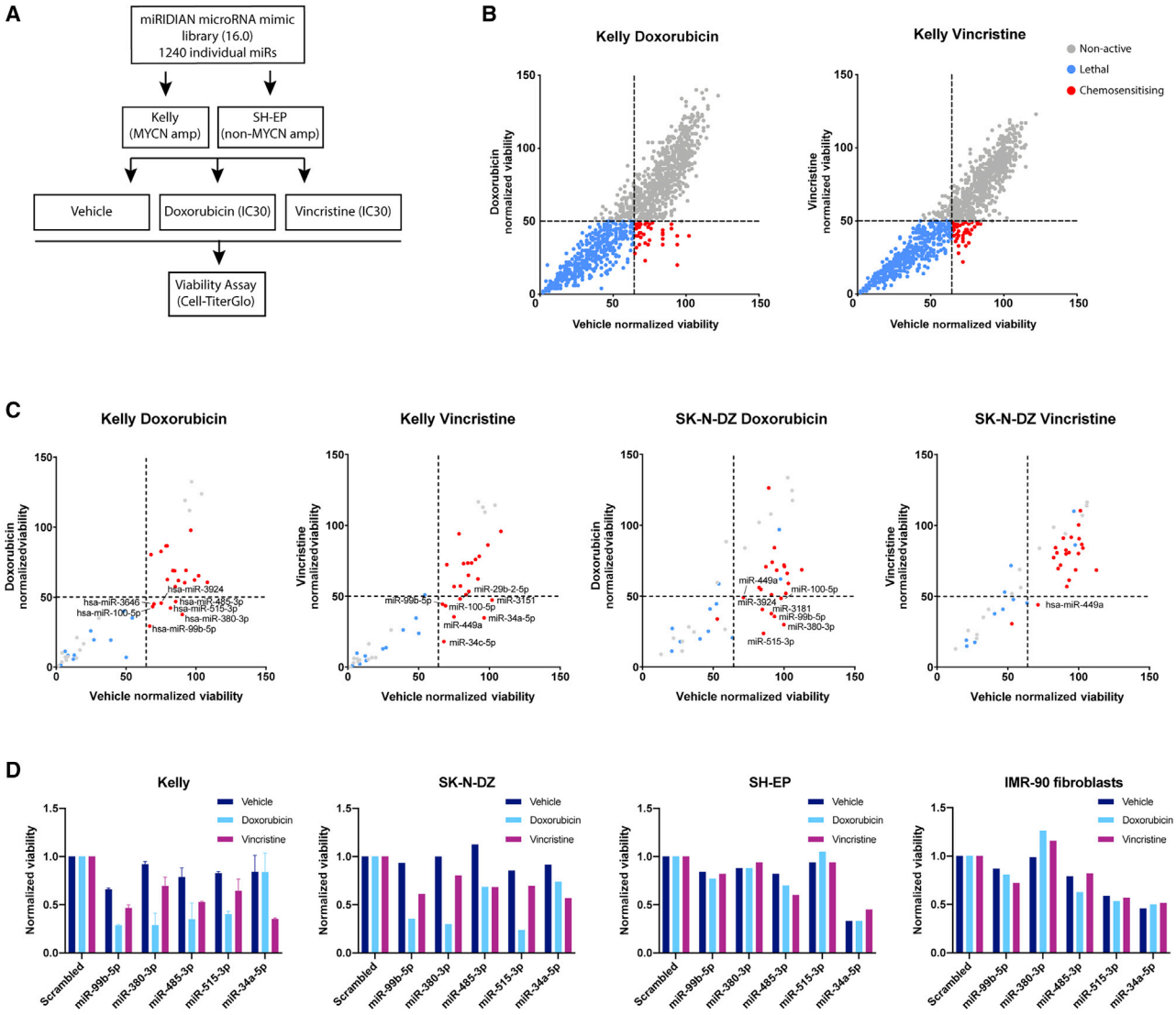

Figure 1. Using high-throughput functional screening to identify chemosensitizing miRNAs in neuroblastoma cell lines

(A) Schematic overview of the miRNA screen in MYCN-amplified Kelly and non-MYCN-amplified (WT) SH-EP neuroblastoma cell lines. (B) Screen results in Kelly cells treated with doxorubicin (left) and vincristine (right) chemotherapy. Plotted are the scrambled-normalized viability values for each miRNA mimic in the vehicle-treated cells (x axis) against drug-treated cells (y axis). Gray indicates non-active, blue indicates lethal (viability <50% in both vehicle- and chemotherapy-treated cells), and red indicates chemosensitizing (vehicle viability >65%, chemotherapy viability <50%) hits. (C) Validation screen results with 48 selected mimics in Kelly and SK-N-DZ cells treated with doxorubicin and vincristine. Hits are colored based on their category in the primary screen as per (B). (D) Bar plots displaying viability of candidate chemosensitizing hits in Kelly, SK-N-DZ, and SH-EP neuroblastoma cell lines as well as IMR-90 fibroblasts in the presence of vehicle, doxorubicin, or vincristine. n = 2, mean ± SD for the Kelly cells representing the primary and secondary validation screen results. See also Figure S1 and Table S1.

cases with copy number variation (CNV) data, miRNA and mRNA sequencing data, and known survival outcomes. All 3 miRNA genes underwent copy-number loss in a subset of patients (Figure 2A). This is consistent with literature reporting that the loci encoding these miRNA genes undergo recurrent deletion in neuroblastoma. The 19q13 locus encoding miR-99b also contains other miRNAs with known tumor-suppressive activity such as let-7e[25] and miR-125a[26] and undergoes the loss of heterozygosity in neuroblastoma at a frequency of ~10%.[27,28] miR-380 and miR-485 are both located on 14q32, which is lost in 20%–25% of neuroblastoma cases.[29–31] Consistently, we found that miR-380 and miR-485 were almost always co-deleted in this cohort (Figure S2A). Deletion of all 3 miRNAs occurred in 12 samples, though there was no cumulative effect on patient survival (Figure S2B).

We next compared our 3 candidate miRNAs' expression in MYCN-amplified with non-MYCN amplified patient tumor samples taken

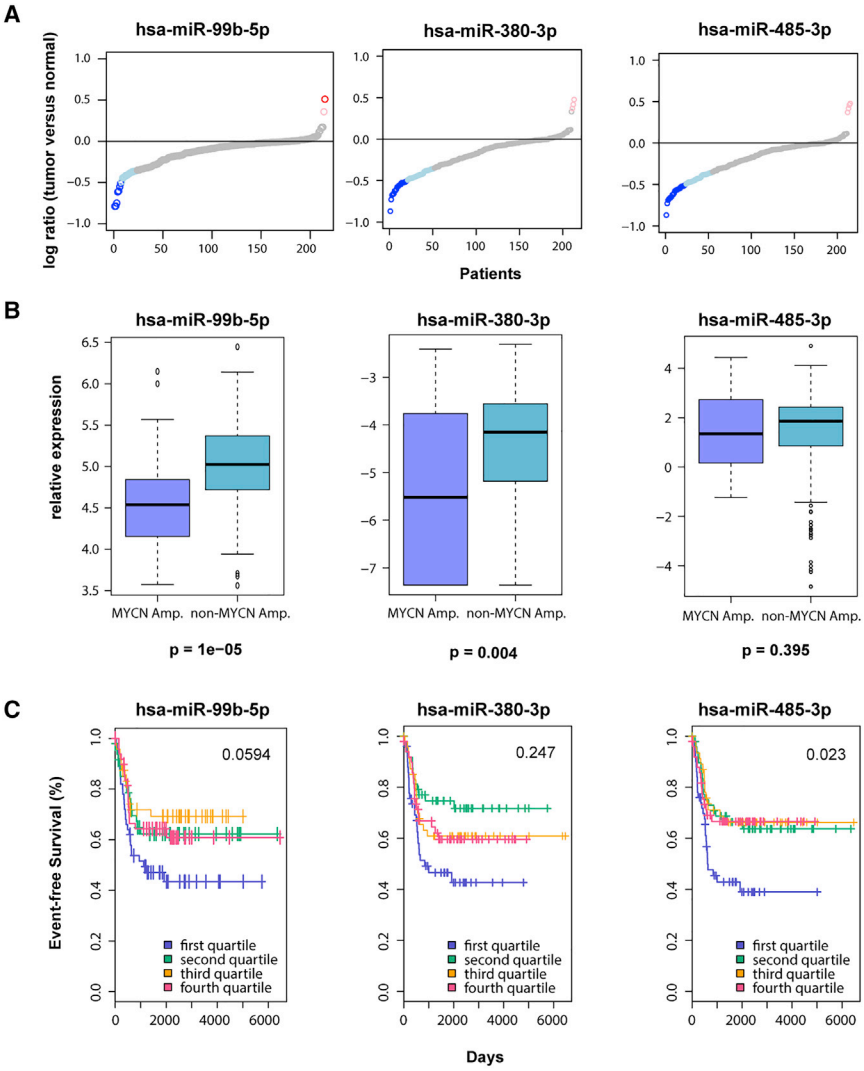

Figure 2. .miR-99b-5p, miR-380-3p, and miR-485-3p positively associated with good prognosis

(A) Copy-number variation of each candidate chemosensitizing miRNA in a cohort of 255 neuroblastoma patients. Blue indicates copy-number loss, and red indicates copy-number gain. (B) Box-and-whisker plots displaying expression of each miRNA in MYCN-amplified and non-MYCN-amplified patients. A Mann-Whitney test was used to calculte significance.(C) Kaplan-Meier analysis (event-free survival) of 250 neuroblastoma patients stratified into quartile expression of each miRNA (first quartile is lowest expression, fourth quartile is highest expression). A Cox proportional-hazards model was applied to calculate significance. See also Figure S2.

at diagnosis. miR-99b-5p and miR-380-3p were both downregulated in MYCN-amplified cases compared with in non-MYCN-amplified cases, though this was not evident for miR-485-3p (Figure 2B). Finally, we correlated miRNA expression with patient survival in this cohort. Patients with the lowest expression had the least favorable outcome in terms of event-free survival (first quartile; Figure 2C).

Taken together, the candidate miRNAs are depleted in high-risk disease (in the case of miR-99b-5p and miR-380-3p), and low expression is associated with poor survival outcomes consistent with our hypothesis that the loss of each of these miRNAs promotes drug resistance. This provided us with a justification to further characterize the function of the miRNAs and to test if replenishing miRNA expression can be used as a strategy to treat models of high-risk neuroblastoma.

Candidate miRNAs decrease proliferation and increase apoptosis in combination with doxorubicin *in vitro*

We focused on doxorubicin-sensitizing miRNAs because most of the validated hits increased sensitivity to doxorubicin and not vincristine (Figures 1C and 1D). To validate the decrease in cell viability in response to doxorubicin, we performed proliferation, cell-cycle, and apoptosis assays in neuroblastoma cell lines transfected with the miRNA mimics. Kelly cells treated with doxorubicin (IC_{30} dose), miR-99b-5p, miR-485-3p, or miR-380-3p alone had a negligible effect on cell growth (Figure 3A). However, the combination of each miRNA with doxorubicin significantly decreased proliferation over the 1-week time course to below 50% compared with that of doxorubicin treatment alone (Figures 3A and S3A). Similar results were observed in the MYCN-amplified COG-N-519 patient-derived cell line model of high-risk neuroblastoma[32] (Figures 3B and S3A).

Cell-cycle distribution of treated Kelly, COG-N-519, and SK-N-DZ cells was determined by analysis of DNA content. Cells treated with doxorubicin had a modest increase in the proportion of cells in the G_2/M phase of the cell cycle (Figures 3C, 3D, and S3B), consistent with published findings.[33] Cells treated with each mimic alone had DNA profiles that resembled control-treated cells, while the combination of each mimic with doxorubicin resulted in an accumulation of cells in G_2/M above doxorubicin alone, particularly for miR-485-3p, which was observed in both Kelly and COG-N-519 cells (Figures 3C and 3D). However, the increase in proportion of cells in G_2/M by miR-485-3p and doxorubicin did not reach statistical significance in the SK-N-DZ cell line (Figure S3B).

It is known that the cytotoxic effects of doxorubicin are more pronounced in cells arrested in the S and G_2/M phases of the cell cycle compared with in the G_1 phase.[33] To test if the miRNAs increased doxorubicin-mediated apoptosis, we performed Annexin V and

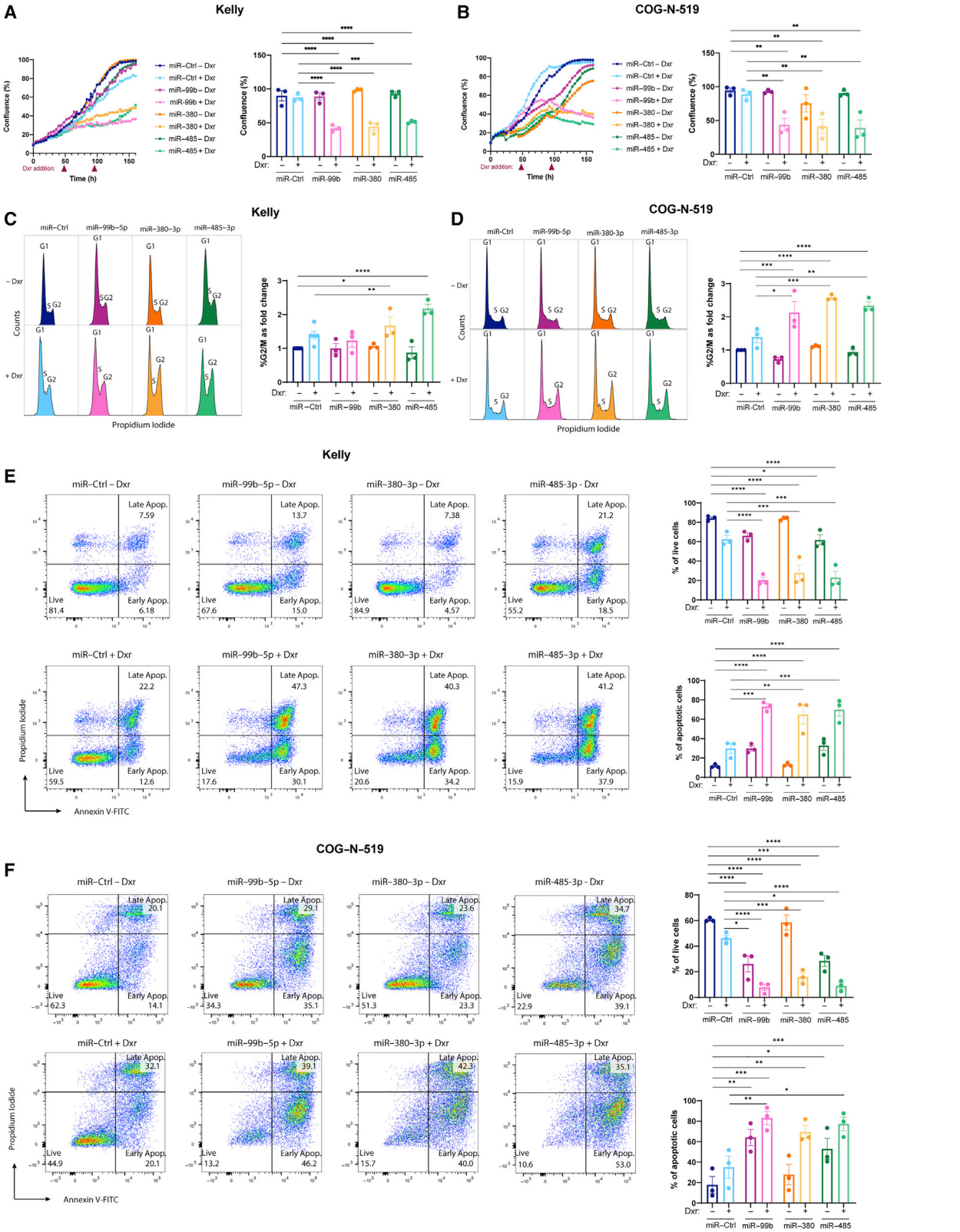

(legend on next page)

propidium iodide (PI) labeling followed by flow cytometry in the same 3 cell lines. The treatment of Kelly and COG-N-519 cells with doxorubicin alone resulted in an increased proportion of apoptotic cells and a decreased proportion of viable cells (Figures 3E and 3F). We also noted that miR-99b-5p and miR-485-3p alone induced apoptosis in Kelly and COG-N-519 cells. However, this was markedly potentiated in cells treated with the candidate miRNAs in combination with doxorubicin (Figures 3E and 3F). A similar trend of decreased viability and increased apoptosis by the miRNAs was observed in doxorubicin-treated SK-N-DZ cells (Figure S3C). Therefore, the 3 candidate miRNAs enhanced the anti-proliferative and pro-apoptotic effects of doxorubicin in multiple neuroblastoma cell lines.

Chemosensitizing miRNA candidates target distinct genes and pathways

To identify the transcriptional targets of the candidate chemosensitizing miRNAs, we performed RNA sequencing (RNA-seq) in Kelly cells. As expected for the overexpression of gene repressors, there were more genes significantly downregulated than upregulated for each miRNA tested compared with the scrambled control (false discovery rate [FDR] <0.05, fold change >1.5) (Figure 4A). We included three non-active miRNAs from the screen (miR-100-3p, miR-1915-3p, and miR-1283) to determine the level of non-specific gene expression changes. The biologically active chemosensitizing miRNAs regulated more genes than did the non-active miRNAs (Figure 4A). In fact, miR-1283 did not have any significant differentially expressed genes compared with the scrambled control (Figure 4A; Table S2).

The top enriched miRNA motif encoded by the repressed genes corresponded to the overexpressed mimic, indicating direct miRNA-mRNA targeting of a subset of the differentially expressed genes (Figure S4A). To determine if the miRNAs had shared targets, we overlapped the genes downregulated by the overexpression of each of the mimics (Figure 4B). Despite the common function of the three miRNAs, only 12 genes (*TMEM30A*, *SCUBE1*, *COL6A6*, *RSPO1*, *ACSF3*, *MAN1C1*, *FGFR3*, *ATP2A3*, *NOTCH2*, *IGHM*, *C15orf56*, and *RP11-428P16.2*) were commonly downregulated, and the majority of the genes were unique. Of the overlapping genes, two are reported to have a role in neuroblastoma tumorigenesis: NOTCH2[34] and FGFR3.[35] NOTCH signaling is known to promote doxorubicin resistance in neuroblastoma cells.[34] We tested whether AZD4547, an inhibitor of FGFR1, -2, and -3, could increase sensitivity to low doses of doxorubicin in Kelly and COG-N-519 cells (Figure S4B). We observed a modest chemosensitizing effect of the AZD4547, suggesting that suppression of FGFR3 signaling may be one of the mechanisms for miRNA-mediated chemosensitivity.

We performed gene set enrichment analysis (GSEA) using Hallmark signatures from the Molecular Signature Database (MSigDB) to investigate which biological pathways were regulated by each miRNA. Common to all 3 candidates was the upregulation of cell-cycle pathways such as "E2F targets", "G_2/M checkpoints", and "mitotic spindle assembly" (Figure 4D), consistent with the perturbation of cell-cycle distribution observed earlier. On the gene level, *CDKN1A* (encoding CDK inhibitor p21) and G2 checkpoint gene *WEE1* were both upregulated by miR-99b-5p treatment (Figure 4C; Table S2). These transcriptomic changes may be responsible for the G_2/M arrest described above (Figures 3C and 3D).

Genes involved in oxidative phosphorylation were downregulated by miR-99b-5p and miR-380-3p (Figure 4D). Targeting cellular metabolism is a possible mechanism for increasing doxorubicin sensitivity, which has been shown in other malignancies such as breast cancer.[36] Other possible transcriptional changes that could explain the increased sensitivity to chemotherapy are the downregulation of the Notch signaling pathway by miR-99b-5p and the downregulation of the epithelial-mesenchymal transition by miR-485-3p, as both of these pathways are known to be associated with chemotherapy resistance in neuroblastoma.[34]

Among the top downregulated genes by miR-99b-5p were chromatin-remodeling gene *SMARCD1,* which was the top differentially expressed gene, and the growth regulatory kinase *MTOR* (Figure 4C; Table S2). Pathway analysis revealed that mTORC1 signaling was also downregulated (Figure 4D). miR-99b-5p is known to suppress *SMARCD1* and *MTOR* in prostate and pancreatic cancer,[37,38] suggesting a conserved role for this miRNA in diverse cancer types. Due to the tumor suppressive gene expression changes elicited by miR-99b-5p, in addition to its anti-proliferative and pro-apoptotic effects in 3 cell lines (Figure 3), its loss of expression in high-risk disease, and its positive correlation with good prognosis (Figure 2), we chose to investigate this miRNA further in different neuroblastoma models.

miR-99b-5p alters gene expression when delivered *in vivo*

We next turned to a more clinically relevant neuroblastoma model to test the feasibility of miR-99b-5p as a candidate therapeutic and to characterize its mechanism of action *in vivo*. To this end, we used

Figure 3. .miR-99b-5p, miR-380-3p, and miR-485-3p potentiate doxorubicin activity *in vitro*

(A and B) Proliferation of Kelly (A) and COG-N-519 (B) cells measured by time-lapse microscopy every 4 h for 7 days using an IncuCyte live cell imager. Cells were transfected with the indicated miRNAs at time 0 and treated with doxorubicin (Dxr) or vehicle at 48 and 96 h as indicated by arrowheads. Representative results from 3 biological replicates shown. Endpoint confluences for each cell line are represented in the bar graphs (n = 3, mean ± SEM). An ordinary one-way ANOVA with Dunnett multiple comparisons test comparing each sample with miR-Ctrl ± doxorubicin was used. (C and D) Representative flow cytometry DNA histograms in Kelly (C) and COG-N-519 (D) cells from 3 independent experiments. Results from 3 biological replicates with bar plots displaying the proportions of cells in G_2/M as a fold change of the miR-Ctrl–doxorubicin condition (n = 3, mean ± SEM). An ordinary one-way ANOVA with Dunnett multiple comparisons test comparing each sample with miR-Ctrl ± doxorubicin was used. (E and F) Flow cytometry analysis of apoptosis in Kelly (E) and COG-N-519 (F) cells after labeling with Annexin V-FITC (apoptosis) and propidium iodide (cell death) and analyzed. Percentage of cells within the quadrant gates are displayed. Representative results from 3 biological replicates shown. Bar graphs display proportion total apoptotic (early and late combined) (n = 3, mean ± SEM). An ordinary one-way ANOVA with Dunnett multiple comparisons test was used to compare each condition with miR-Ctrl ± doxorubicin. See also Figure S3.

(legend on next page)

the COG-N-519 patient-derived xenograft (PDX) model derived from a patient with high-risk MYCN-amplified disease.[32] Tumors were grown subcutaneously in NSG mice and injected with Star-poly(oligo(ethylene glycol) methacrylate) (POEGMA) nanoparticles complexed to 2′-O-Methyl (2′-OMe)-modified miRNA mimics to increase their *in vivo* stability and to allow them to internalize into cells.[39,40] To test if we could deliver the mimics, mice were injected with control miRNA or miR-99b-5p nanoparticles every 3 days for 1 week. Tumor growth was measured, and tumors were harvested for gene expression analysis 24 h following the last injection. miR-99b-5p had a modest growth inhibitory effect, though the reduction was not statistically significant (Figure 5A). Furthermore, immunohistochemical staining of these tumors for markers of proliferation (Ki67) and apoptosis (cleaved caspase 3) did not reveal any differences between miRNA control (miR-Ctrl) and miR-99b-5p tumors (Figure S5A). This is consistent with miR-99b-5p transfection having a modest effect on proliferation in the absence of chemotherapy in the matched patient-derived cell line (Figure 3B). It is also possible that the treatment time was not sufficient to produce a measurable effect on proliferation and apoptotic markers *in vivo*. Quantitative RT-PCR (qRT-PCR) revealed a ∼40-fold increase in miR-99b-5p expression (Figure 5B), confirming that the mimic was delivered to the tumor.

We next analyzed gene expression changes by RNA-seq. Differential gene expression analysis revealed 713 upregulated and 472 downregulated genes in miR-99b-5p-treated tumors compared with in controls (FDR <0.05, fold change >1.5) (Table S3). GSEA analysis revealed that upregulated genes were involved in processes relating to development and neuronal differentiation such as “developmental growth involved in morphogenesis”, “neuron projection guidance”, and “axon development” (Figure 5C). Genes involved in proliferation and DNA damage such as “DNA replication”, “DNA recombination”, “double-strand break repair”, and “cell-cycle checkpoint” were negatively regulated (Figure 5C). Together, this suggests that treatment of the tumors with miR-99b-5p rewired the transcriptome to a more differentiated and less proliferative state. We expect that these gene expression changes represent both direct and indirect effects of the week-long treatment with the miRNA mimic, which is supported by the fact that the predicted miR-99b-5p motif was not enriched in the downregulated genes (Figure S5B) and that there were more genes upregulated than downregulated (Table S3).

miR-99b-5p targets essential neuroblastoma genes *LIN28B* and *PHOX2B*

To stringently identify genes repressed by miR-99b-5p, we performed an additional RNA-seq experiment in COG-N-519 cells *in vitro* (Table S4). We then identified the commonly downregulated genes from the three RNA-seq experiments: the two *in vitro* experiments where Kelly and COG-N-519 cells were transfected with miR-99-5p for 48 h and the *in vivo* experiment where COG-N-519 PDX tumors were treated with miR-99b-5p nanoparticles for 7 days. There were 8 genes downregulated by miR-99b-5p in all three experiments (*LIN28B*, *TRIP13*, *PHOX2B*, *ARHGAP29*, *MYCBP*, *SALL4*, *RP11-161D15.3*, and *EFNB2*) (Figure S5C). On the pathway level, genes involved in mTOR signaling and cholesterol homeostasis were commonly downregulated by miR-99b-5p in Kelly and COG-N-519 cells (Figures 4D and S5D).

We selected key neuroblastoma oncogenes, *LIN28B* and *PHOX2B*, downregulated in all three datasets for further validation. LIN28B is an RNA-binding protein that promotes tumorigenesis by inhibiting biogenesis of the let-7 family of tumor-suppressive miRNAs.[19] PHOX2B is a homeodomain transcription factor essential for the survival and differentiation of the sympathetic lineage and is a germline disposition gene and lineage oncogene in neuroblastoma.[41–43] Inspection of public data from the project Achilles CRISPR knockout screen demonstrated that both of these genes are essential for neuroblastoma cell survival[44,45] (Figure S5E). Repression of *PHOX2B* and *LIN28B* by miR-99b-5p was validated by qRT-PCR (Figure 5D). qRT-PCR was also performed in the matched PDX cell line and Kelly and SK-N-DZ cells 48 h post transfection with control or miR-99b-5p. *LIN28B* was consistently downregulated in all 3 cell lines, and *PHOX2B* was significantly downregulated in Kelly cells and trended toward downregulation in COG-N-519 and SK-N-DZ cells (Figure 5D). To confirm repression on the protein level, western blotting was conducted on the same cell lines 72 h post transfection (Figure 5E). Across four biological replicates, we observed a significant downregulation of the PHOX2B protein in each cell line, a downregulation of LIN28B in SK-N-DZ cells, and a trend toward repression in COG-N-519 and Kelly cells.

We next investigated whether these targets were responsible for miR-99b-5p-mediated chemosensitivity. To this end, we knocked down LIN28B and PHOX2B with siRNA, either alone or together, and assayed cell viability and proliferation in the presence and absence of doxorubicin. Western blotting confirmed knock down by the siRNA to a similar level as miR-99b-5p (Figures 5E and S5F). In parallel, we overexpressed miR-99-5p to test whether siRNA-mediated depletion of LIN28B and PHOX2B could phenocopy the effects of the mimic. Knock down of PHOX2B and LIN28B did not affect viability in the untreated cells (Figure 5F); however, knock down of PHOX2B and LIN28B either alone or in combination did partially recapitulate the

Figure 4. .Chemosensitizing miRNAs target distinct genes and pathways

(A) RNA-seq of differentially expressed genes up- or downregulated (FDR <0.05, fold change >1.5) by each indicated miRNA compared with the scrambled control in Kelly cells. Four biological replicates were performed. (B) Venn diagrams showing overlapping genes regulated by each chemosensitizing miRNA. Blue represents downregulated and orange represents upregulated gene lists. (C) Volcano plots displaying statistical significance (y axis) over fold change (x axis) for each gene comparing chemosensitizing miRNA with scrambled control. In purple are significantly differentially expressed genes (FDR <0.05 and fold change > 1.5), and gray are non-significant genes. (D) Gene set enrichment analysis results using the Hallmark gene set from the Molecular Signature Database. Orange bars represent upregulated and blue bars represent downregulated gene sets. See also Figure S4 and Table S2.

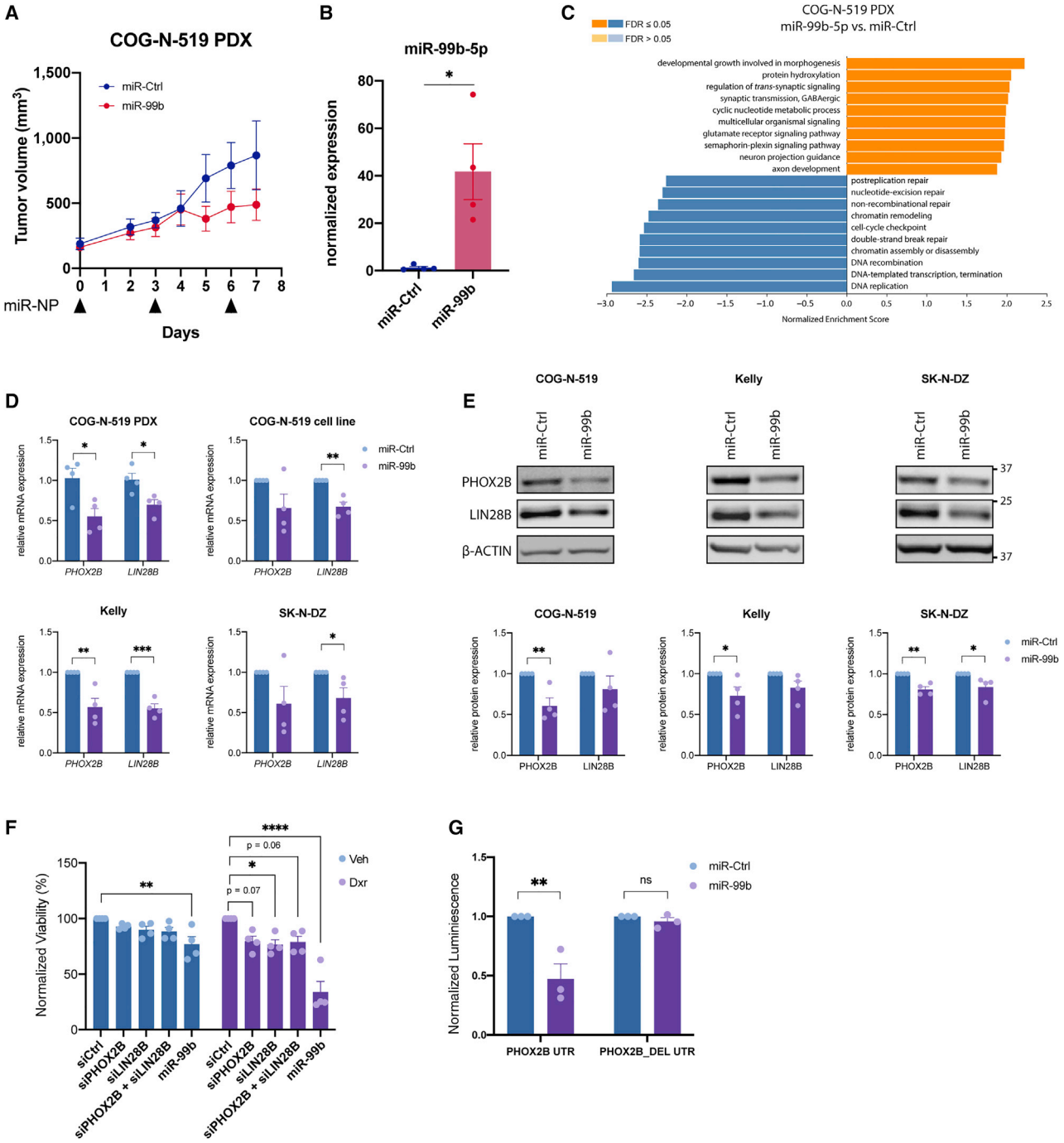

Figure 5. .miR-99b targets PHOX2B and LIN28B

(A) Growth curves of subcutaneous COG-N-519 PDX tumors. miR-99b-5p or control miR-1283 (miR-Ctrl) complexed to nanoparticles (miR-NPs) were injected intratumourally at the indicated times (n = 4, mean ± SEM). (B) qRT-PCR analysis of miR-99b-5p expression in PDX tumors collected 24 h after the last miRNA injection (n = 4, mean ± SEM). An unpaired two-tailed t test was used to test significance. (C) Gene set enrichment analysis results using the Gene Ontology Biological Processes gene set from the Molecular Signature Database. Orange bars represent upregulated and blue bars represent downregulate gene sets. (D) qRT-PCR analysis for *PHOX2B* and *LIN28B* in COG-N-519 PDX tumors following 1 week of miR-99b-5p treatment or following 48 h of miR-99b-5p transfection in COG-N-519, Kelly, and SK-N-DZ cell lines (n = 4, mean ± SEM). An unpaired two-tailed t test was used to test significance. (E) Western blot analysis for PHOX2B and LIN28B in Kelly, COG-N-519, and SK-N-DZ cell lines transfected with miR-Ctrl or miR-99b-5p after 72 h. Representative images from 4 experiments shown. Below are the densitometry analysis of the protein bands normalized to β-actin (n = 4, mean ± SEM). An unpaired two-tailed t test was used to test significance. (F) CellTiter-Glo viability of COG-N-519 cells transfected with the indicated siRNAs

(legend continued on next page)

reduction in viability in doxorubicin-treated cells by miR-99b-5p (Figure 5F). These results were corroborated in the proliferation assay; in the absence of chemotherapy, the depletion of PHOX2B and LIN28B did not appreciably reduce proliferation, but in the context of chemotherapy treatment, knock down of PHOX2B and LIN28B reduced proliferation by approximately 20%–60% (Figure S5G). Together, these data suggest that the inhibition of LIN28B and PHOX2B may be partially responsible for miR-99b-5p's chemosensitizing activity. As miRNAs target hundreds of genes, we hypothesize that multiple targets acting in concert are required for miR-99b-mediated chemosensitization.

To determine if miR-99b-5p directly targeted *PHOX2B* and *LIN28B*, we used miRanda-mirSVR[46] and Diana-MicroT-CDS[47] miRNA prediction tools to search for miR-99b-5p recognition sites in the 3′ UTR of the two transcripts. The *PHOX2B* 3′ UTR contained a predicted miR-99b-5p 6-mer seed match (ACGGGU) (Figure S5H). No predicted motif was identified for LIN28B. To experimentally validate the putative direct targeting of PHOX2B by miR-99b-5p, we synthesized and cloned the conserved 518 bp region containing the predicted binding site of the PHOX2B 3′ UTR[48] downstream of luciferase and used this construct for performing luciferase reporter assays in HEK-293T cells. This was also done for the PHOX2B 3′ DEL UTR, engineered to lack the predicted seed sequence. Co-transfection of cells with the PHOX2B 3′ UTR luciferase construct and miR-99b-5p resulted in the repression of luciferase activity (Figure 5G). However, the activity of the PHOX2B 3′ DEL UTR was not impacted by miR-99b-5p transfection (Figure 5G), demonstrating that miR-99b-5p targets PHOX2B directly through its interaction with the predicted seed sequence.

DISCUSSION

There is an outstanding need for improved and safer treatment options for high-risk neuroblastoma patients. miRNAs are critical regulators of neuroblastoma tumorigenesis and represent an exciting new class of cancer therapeutics. A major challenge in the development of miRNA-based drugs is determining which miRNAs make the most suitable therapeutic candidates in a given cancer type. Ooi and colleagues used miRNA-mRNA interaction modeling to uncover tumorigenic miRNA gene networks and identified miR-204 as a neuroblastoma tumor suppressor, which functions through the direct inhibition of MYCN.[20] Using high-throughput screening, several miRNAs lethal to neuroblastoma cells including miR-101-3p, miR-202-3p, and miR-19-b-1-5p have also been identified.[21]

Combination therapy is more likely to lead to durable cancer control, and new therapeutics are generally first combined with standard-of-care therapies in clinical trials. We therefore sought to identify miRNAs that could sensitize neuroblastoma cells to the standard-of-care chemotherapy drugs doxorubicin and vincristine. We hypothesize that these miRNAs will be less toxic, as they target pathways involved in the response to chemotherapy rather than essential functions of the cell. Here, we identify miR-99b-5p, miR-380-3p, and miR-485-3p as doxorubicin-sensitizing miRNAs in multiple models of high-risk neuroblastoma. The fact that these miRNAs only sensitized the cells to doxorubicin and not to the microtubule disruptor vincristine suggests that their synergistic action is not via generic survival pathways but rather is specific to DNA-damaging agents. This is supported by the low toxicity of these miRNAs in three lineages of non-transformed cells (epithelial MCF10A, mesenchymal fibroblasts, and cardiomyocytes). These miRNAs are lowly expressed in poor-prognosis disease and were shown to alter the transcriptome to reduce proliferation, induce cell-cycle arrest, and cause apoptosis when combined with IC_{30} doses of doxorubicin.

Each of the 3 candidates have reported tumor-suppressive roles in different cancer types. For example, miR-99b-5p has demonstrated tumor-suppressive functions in prostate,[37] gastric,[49] lung,[50,51] and colorectal[52] cancers. A tumor-suppressive role for miR-485-3p has been described in glioblastoma,[53,54] breast cancer,[55] and leukemia.[56] However, these two miRNAs have not been investigated in neuroblastoma.

miR-380-3p has been shown to modestly increase apoptosis and sensitize murine neuroblastoma cells to the poisonous herbicide paraquat.[57] This is perhaps consistent with its ability to sensitize human neuroblastoma cells to chemotherapy, as demonstrated here. Interestingly, miR-380-5p, the alternate mature miRNA arm derived from the same miR-380 precursor, is oncogenic in neuroblastoma and functions through the suppression of p53.[17] A recent study in gastric cancer demonstrated opposing tumor-suppressive and oncogenic functions for miR-574-3p and miR-574-5p, respectively.[58] The two mature miRNA arms were inversely expressed, and the arm balance was partially mediated by the presence of their target mRNA.[58] Further studies should determine if such a relationship for tumor-suppressive miR-380-3p and oncogenic miR-380-5p exists in neuroblastoma.

Our RNA-seq analysis revealed that each of the 3 candidates had few overlapping targets. Relevant genes commonly downregulated by the 3 candidate chemosensitizing miRNAs were *FGFR3* and *NOTCH2*. Fibroblast growth factor receptors (FGFRs) are a family of tyrosine kinase receptors that are often deregulated in cancer, resulting in enhanced proliferation, invasiveness, and survival.[59] A recent study demonstrated that several neuroblastoma cell lines were sensitive to FGFR inhibitors.[35] While we corroborated that FGF inhibition was cytotoxic to neuroblastoma cells, we observed only a modest increase in sensitivity to doxorubicin with the addition of an FGFR1, -2, and -3

and miRNAs and treated with doxorubicin. Viability was measured following 1 week of treatment (n = 4, mean ± SEM). An ordinary one-way ANOVA with Dunnett multiple comparisons test comparing each sample with the scrambled control ± doxorubicin was used to test significance. (G) HEK-293T cells were co-transfected with miR-Ctrl or miR-99b-5p mimics and PHOX2B reporter plasmid encoding either WT (PHOX2B UTR) or mutated 3′ UTR lacking the predicted miR-99b-5p binding site (PHOX2B_DEL UTR). Twenty-four h later, the cells were subjected to the dual luciferase assay. The graph plots transfection-normalized luciferase signals relative to the miR-Ctrls (n = 3, mean ± SEM). An unpaired two-tailed t test was used to test significance. See also Figure S5.

inhibitor. NOTCH2 is one of the core transcription factors that defines the mesenchymal/neural-crest-like neuroblastoma epigenetic state.[34,42] Induction of the related transcription factor NOTCH3 in SH-SY5Y neuroblastoma cells resulted in increased resistance to DNA-damaging chemotherapy including doxorubicin.[34] Further studies are needed to validate targeting of the Notch pathway by these miRNAs and whether this represents a common mechanism for reprogramming neuroblastoma cells to a less chemoresistant state.

We delved further into the mechanism of miR-99b-5p to show that it targets *LIN28B* and *PHOX2B* both *in vitro* and *in vivo*. Furthermore, we show that miR-99b-5p targets *PHOX2B* directly via binding to its 3′ UTR, whereas the suppression of *LIN28B* likely occurs through an indirect mechanism, as we did not detect a predicted miR-99b-5p binding site. PHOX2B is a member of the core regulatory circuitry of transcription factors that defines adrenergic neuroblastoma identity and is required for neuroblastoma cell survival.[41–43,60] This transcription factor has not yet been implicated in chemotherapy resistance. The proto-oncogene LIN28B promotes neuroblastoma stemness and tumorigenesis[19,61] and has been implicated in doxorubicin resistance in a sarcoma cell line.[62] Consistent with LIN28B's role in promoting stemness and inhibiting differentiation, we observed an upregulation of neuronal differentiation gene sets in our PDX model treated with miR-99b-5p. We hypothesize that the loss of miR-99b-5p gives rise to high-grade undifferentiated disease through the upregulation of stem cell factors such as LIN28B. Interestingly LIN28B can act as a transcription co-factor and occupies the *PHOX2B* super enhancer, and PHOX2B binds to the *LIN28B* super enhancer.[63] This suggests that LIN28B and PHOX2B upregulate each other's expression in a positive feedforward loop. Nucleic acid binding proteins are notoriously difficult to target using small-molecule inhibitors, thus targeting these factors with miR-99b-5p could be a way to break the feedforward loop to render neuroblastoma cells more susceptible to chemotherapy.

A strength of using miRNAs as therapeutics is their ability to target multiple different transcripts, which could bypass resistant mechanisms from emerging by targeting multiple compensatory pathways.[14] Depletion of miR-99b-5p targets PHOX2B, and LIN28B could only partially phenocopy the overexpression of miR-99b-5p, which indicates that other genes are likely to be involved in promoting chemosensitivity. We found that cholesterol homeostasis and mTOR signaling were the top pathways downregulated by miR-99b-5p in two different neuroblastoma cell lines. Interestingly, statins can enhance the effects of doxorubicin in cancer cells through inhibiting cholesterol synthesis.[64–66] The mTOR pathway has also been implicated in doxorubicin resistance.[67,68] We postulate that the suppression of multiple pathways by miR-99b-5p collectively contributes to increasing doxorubicin sensitivity. A limitation of using transcriptomic data to study miRNA function is that miRNAs also work through inhibiting translation, meaning that miRNA targets may be missed in our analysis.

Future studies are needed to test the *in vivo* efficacy of these miRNAs in combination with chemotherapy. This could be achieved using nanoparticle delivery vectors or by using inducible transgenic models. The translation of miRNAs into the clinic has been hindered by pharmacological challenges involved in the systemic delivery of miRNA-based drugs to the target site. Fortunately, significant advances have been made in this space. For example, the company EnGeneIC is developing bacteria-derived minicells loaded with tumor-suppressive miR-16 mimics for the treatment of plural mesothelioma.[40,69] These so-called TargomiRs successfully completed phase I clinical trials and will soon progress to phase II.

In conclusion, we have uncovered miR-99b-5p, miR-380-3p, and miR-485-3p as therapeutic candidates that have the potential to be used in conjunction with a safer and more tolerable dose of chemotherapy for treating high-risk neuroblastoma.

MATERIALS AND METHODS

Cell culture growth conditions

Kelly, SH-EP, and SK-N-DZ established neuroblastoma cell lines and neuroblastoma patient-derived COG-N-519 cells were obtained from the Childhood Cancer Repository of the Children's Oncology Group, Texas Tech University Health Sciences Center, Lubbock, TX, USA. IMR-90 and HEK-293T cell lines were obtained from the American Type Culture Collection (ATCC). Kelly and SH-EP cells were grown in Roswell Park Memorial Institute (RPMI) medium (Gibco) supplemented with 10% fetal bovine serum (FBS; Hyclone). SK-N-DZ and HEK-293T cells were grown in Dulbecco's modified Eagle's medium (DMEM; Gibco) supplemented with 10% FBS. COG-N-519 cells were grown in Iscove's modified Dulbecco's medium (IMDM; Gibco) supplemented with 20% FBS and 1× insulin-transferrin-sodium selenite (ITS; Sigma). IMR-90 cells were grown in Earl's MEM (Gibco) supplemented with 10% FBS, 1× Non-Essential Amino Acids (Gibco), and 1× Sodium Pyruvate (Gibco).

High-throughput miRNA screening

Primary and validation screening in neuroblastoma cell lines was performed as described previously.[21] Briefly, cells were reverse transfected in a 384-well plate with 25 nM Dharmacon miRNA mimic libraries (v.16.0) using DharmaFECT 1 transfection reagent (Dharmacon RNAi Technologies, Horizon Discovery). Media was changed after 24 h, and at 48 h, media containing doxorubicin or vincristine chemotherapy (IC_{30} doses in Table S5) or vehicle control was added. Chemotherapy was replenished after a further 48 h, and at 144 h post transfection, cell viability was measured using the CellTiter-Glo (CTG) luminescent assay (Promega) and read on a Cytation 3 plate reader (BioTek). All screens were performed in technical duplicate. Values were normalized to the ON-TARGETplus siRNA SMARTpool (Dharmacon catalog number [cat. #] 001810-10-50) control on a per plate basis, and duplicate plate values were averaged. IC_{30} values were determined by non-linear regression analysis by Graphpad Prism 9 software.

Clinical cohort

Neuroblastoma tumor miRNA expression data and DNA copy-number data were previously published.[70,71] Segments of equal copy-number

levels were determined using the Circular Binary Segmentation (CBS) algorithm. For each miRNA, the CN status (expressed as a log ratio) was established based on miRNA genome coordinates (obtained from miRbase). Patient tumor miRNA expression data was compared between tumors with and without MYCN amplification using a Mann-Whitney test. To assess the association between miRNA expression data and patient survival, patients were separated into four groups according to miRNA expression quartiles to generate Kaplan-Meier survival plots. A Cox proportional-hazards model was applied to calculate significance.

Proliferation assay

1.4×10^4 Kelly or COG-N-519 cells were seeded in 48-well plates and transfected with 25 nM miRNA or 40 nM siRNA using DharmaFECT 1 transfection reagent (Dharmacon) (Table S6). Media were changed 24 h later. Doxorubicin was added 48 and 96 h after transfection. Cells were grown for 7 days, and phase-contrast confluence was monitored by time-lapse microscopy every 4 h using an Incuyte ZOOM system. Experiments were repeated 2–3 times.

Cell-cycle assay

Kelly, COG-N-519, and SK-N-DZ cells were seeded in 6-well plates and transfected with miRNA and treated with doxorubicin as described above. 24 h following doxorubicin treatment, cells were trypsinized and fixed in 70% ethanol overnight at 4°C. Cells were stained with 10 μg/mL PI and treated with 0.5 mg/mL RNaseA for up to 5 h. Flow cytometry was performed using a BD FACSCanto II flow cytometer and analyzed using FlowJo v.10. The Dean-Jett-Fox model was used to gate DNA histograms into G_1, S, and G_2/M phases. The experiment was repeated 3 times.

Apoptosis assay

Kelly, COG-N-519, and SK-N-DZ cells were seeded, transfected, and treated with doxorubicin as described above. Adherent and floating cells were harvested 72 h following doxorubicin treatment and stained using the eBioscience Annexin V-FITC Apoptosis Detection Kit (Thermo Fisher Scientific). Flow cytometry was performed on a BD FACSCanto II flow cytometer and analyzed using FlowJo v.10. Experiments were repeated 3 times.

Cell viability assay

COG-N-519 or Kelly cells were seeded in white 96-well plates and transfected with 25 nM miRNA or 40 nM siRNA using DhamaFECT1 (Dharmacon) in technical triplicate. Cells were treated with doxorubicin (Table S3) 48 and 96 h following transfection, and cell viability was measured using the CTG luminescent assay (Promega) on day 7. For the FGFRi experiment, cells were treated with 5 μM AZD4547. Experiments were performed 3–4 times.

RNA-seq of cell lines

6×10^5 Kelly or COG-N-519 cells were seeded in 6-well plates and transfected with 25 nM miRNA. Media were changed after 24 h, and cells were collected for RNA isolation the following day (48 h after miRNA transfection). RNA was extracted using the Qiagen miRNeasy mini kit (Qiagen). RNA concentration and purity were measured using a NanoDrop ND-1000 spectrophotometer (NanoDrop Technologies), and integrity was verified using an Agilent Bioanalyser 2100 with the 6000 Nano Assay (Agilent Technologies) or TapeStation with an RNA ScreenTape (Agilent Technologies). Libraries were generated using the Illumina TruSeq Stranded mRNA Library Prep Kit (Illumina) with 1 μg input RNA. cDNA libraries from Kelly cells were sequenced on a HiSeq 2500 system (high output mode) (Illumina), with 125 bp paired-end reads. cDNA libraries from COG-N-519 cells were sequenced using a NovaSeq 6000 SP, with 100bp paired-end reads. Four biological replicates were performed for each experiment.

RNA-seq of PDX tumors

Snap-frozen tissue pieces of COG-N-519 PDX tumors were collected 24 h following the last miRNA-nanoparticle injection. RNA was isolated from tissue using a TissueLyser II (Qiagen) and the Qiagen miRNeasy mini kit (Qiagen). RNA concentration and purity were measured using a NanoDrop ND-1000 spectrophotometer (NanoDrop technologies), and integrity was verified using a LabChip GX 24 (PerkinElmer). The KAPA RNA HyperPrep kit was used with 1 μg input RNA to generate cDNA libraries. Library concentrations were determined using the Qubit HS Assay Kit (Thermo Fisher Scientific) and sequenced on the NextSeq system (high output mode) with 150 bp paired-end reads. Three tumors from each treatment group were analyzed.

RNA-seq analysis

FastQC was used to remove poor quality reads and to trim Illumina sequencing adapters.[72] Reads were aligned to the human reference genome HG19 using STAR ultrafast universal RNA-seq aligner.[73] RSEM accurate transcript quantification for RNA-seq data was used to generate a gene read count table and to filter genes with read counts of 0.[74] Differential gene expression analysis was performed using the limma R package.[75] Pre-ranked GSEA was performed using WebGestalt 2019.[76]

Quantitative real-time PCR analysis

RNA was extracted from cells or tissue as described above. Reverse transcription was performed using the TaqMan MicroRNA Reverse Transcription Kit to detect miRNAs and Transcriptor First Strand cDNA Synthesis Kit (Roche) to detect mRNA. TaqMan probes (Thermo Fisher Scientific) listed in Table S7 were used to analyze mRNA expression levels using a QuantStudio 7 Flex Real-Time PCR System. miRNA expression was normalized to RNU48, and mRNA expression normalized to GAPDH. Experiments were repeated 4 times.

Western blotting

Cells grown in 6-well plates were scraped in radioimmunoprecipitation assay (RIPA) buffer supplemented with 1 mM DTT, a protease inhibitor cocktail, and phosphatase inhibitors (Sigma-Aldrich). Protein concentration was quantified using the Pierce BCA Protein Assay Kit (Thermo Fisher Scientific). Protein lysates (20–25 μg protein) were mixed with NuPage loading buffer and a reducing agent (Life

Technologies) and denatured by heating at 85°C for 5 min. Samples were run on pre-cast 4%–12% Bis/Tris gels (Life Technologies) in MOPS running buffer (Life Technologies). Protein was transferred to a 0.45 μm polyvinylidene fluoride (PVDF) membrane (Merck Millipore) using BioRad transfer modules in transfer buffer (25 mM Tris, 192 mM Glycine, 20% Methanol). Membranes were blocked in Odyssey blocking buffer (LI-COR) for 1 h at room temperature then incubated in a primary antibody diluted in 5% BSA/TBS overnight at 4°C. The following antibodies were used for western blotting: LIN28B (1:1,000, CST 4196S), PHOX2B (1:500, Santa Cruz sc-376997), and β-actin (1:1,000, Sigma-Aldrich A5441). Fluorescent secondary antibodies conjugated to IRDye680 or IRDye800 (LI-COR) diluted in Odyssey Blocking Buffer (1:15,000) were used for detection. Images were acquired using an Odyssey CLx (LI-COR) or a ChemiDoc MP (Biorad) imaging system. Band density was quantified using LI-COR ImageStudio software, with normalization to β-actin. Experiments were repeated 4 times.

Preparation of miRNA mimics nanoparticle complexes

miRNA mimics were purchased from Shanghai GenePharma and contained 2′-OMe modifications on the first and last 4 bases of the sense strand to protect the duplex from degradation (Table S6).[40] Star-POEGA nanoparticles were synthesized and complexed to mimics as described in Teo et al.[39] Briefly, 25 μg miRNA mimic and 75 μg nanoparticles were mixed in 1% glucose solution and incubated for 5 min at room temperature in 70 μL injection volumes and stored at 4°C for up to 1 week.

Mouse experiments

Female NOD-SCID IL2Rγ-null (NSG; ID: NOD.CgPrkdcIL2rgSzJAusb) mice at 5–6 weeks of age were purchased from Animal Resources Center (Canning Vale, WA, Australia). Animals were housed in a specific-pathogen-free environment in Techniplast research animal cages with filter tops and a floor area of 400 cm^2 with 2–6 mice/cage and under 12:12 light/dark cycles. Bedding, Enviro-dry, and igloos were provided for environmental enrichment. Irradiated rat and mouse breeder cubes and water were provided ad libitum. Mice were acclimatized for a week prior to experimentation. All animal experiments were conducted at the Children's Cancer Institute under the ethics approvals 17/53B and 20/25B, as approved by the UNSW Animal Care and Ethics Committee (Sydney, NSW, Australia).

To assess miRNA uptake and activity, COG-N-519 PDX cells (1×10^6cells/mouse) were mixed in RPMI (Life Technologies) and growth-factor-reduced Matrigel (Corning, Corning, NY, USA) at an equal volume ratio and implanted subcutaneously into the flank of mice. Once each tumor reached 100 mm^3, mice were placed into one of two groups (4 mice per group). The miRNAs were given intratumorally as a nanoparticle complex (25 μg miRNA + 75 μg nanoparticles) under light anesthesia every 3 days for 7 days. Tumor volume was measured by Vernier calipers using the following formula: tumor volume = length × width × height/2. Mice were euthanized 24 h following the last injection, and tumors were harvested for subsequent molecular analyses.

Immunohistochemistry (IHC)

IHC staining was performed on 4 μm sections of formalin-fixed paraffin-embedded (FFPE) tissue using a BOND RX autostainer with primary antibodies for Ki67 (Thermo #RM-9106 clone SP6, 1:500) and cleaved caspase 3 (CST #9964 clone 5A1E, 1:200). Whole sections were imaged using an Aperio Slide Scanner, and images quantified using QuPath software.

miRNA luciferase reporter assay

miRanda-mirSVR[46] and Diana-MicroT-CDS[47] miRNA prediction tools were used to identify a predicted miRNA binding site for miR-99b-5p in the PHOX2B 3′ UTR. The last 518 bp of the PHOX2B 3′UTR (NCBI Reference Sequence: NM_003,924.4; see Supplemental information) flanked by XhoI and NotI recognition sites were synthesized by IDT as a gBlock sequence. A mutated sequence lacking the predicted miR-99b-5p binding site was also synthesized (see Supplemental information). gBlock inserts and recipient psiCHECK2 (Promega) vector DNA were digested with XhoI and NotI restriction enzymes (NEB) to generate sticky ends and purified using Wizard SV Gel and PCR Clean-Up columns (Promega). Digested DNA was ligated at insert:vector ratio of 3:1 using T4 DNA ligase (NEB), and the resulting ligation reaction was used to transform DH5α competent *E. coli* cells in the presence of 100 μg/μL Ampicillin (Sigma). Ten colonies per plasmid were selected for colony PCR to screen for successfully transformed clones using the following primers (forward [Fw]: 5′-CATCAAGAGCTTCGTGGAGC-3′, reverse [Rv]: 5′-GAAGACTCATTTAGATCCTCACAC-3′). Selected colonies were grown in Luria-Bertani (LB) broth containing 100 μg/μL Ampicillin and plasmid DNA isolated using the Qiagen plasmid plus maxi kit. Sanger sequencing using the above primers was used to verify the sequence of the plasmids.

To perform the luciferase assays, 2×10^4 HEK93T cells were seeded in white 96-well plates. The following day, 12.5 ng reporter plasmid and 50 nM miRNA were co-transfected using Lipofectamine 3000 (Thermo Fisher Scientific) in technical triplicates. After 24 h, the Dual-Luciferase Reporter Assay (Promega) was performed as described previously.[21] Renilla luciferase activity was normalized to the firefly luciferase signal to normalize for transfection efficiency. The experiment was repeated 3 times.

Statistics

Statistical analysis was performed using GraphPad Prism 9 using the indicated tests. When comparing 2 groups, an unpaired two-tailed t test was used, and when comparing 3 or more groups, an ordinary one-way ANOVA with Dunnett's multiple comparisons test was used, comparing each test condition with the control. *$p < 0.05$, **$p < 0.01$, ***$p < 0.001$, and ****$p < 0.0001$.

Data availability

Kelly RNA-seq data is available on the GEO repository (GEO: GSE175729). COG-N-519 RNA-seq data is available on the European Genome-phenome Archive (EGA) (EGA: EGAD00001008035 and EGAD00001007754).

SUPPLEMENTAL INFORMATION

Supplemental information can be found online at https://doi.org/10.1016/j.ymthe.2022.01.004.

ACKNOWLEDGMENTS

H.H, E.D., and A.S were supported by The Kids' Cancer Project, Deborah and John McMurtrie, and The Ross Trust. The Victorian Center for Functional Genomics (K.J.S. and I.N.) is funded by the Australian Cancer Research Foundation (ACRF), Phenomics Australia (PA) through funding from the Australian Government's National Collaborative Research Infrastructure Strategy (NCRIS) program, and the Peter MacCallum Cancer Centre Foundation. This work was supported by the Children's Cancer Institute, which is affiliated with the University of New South Wales (UNSW Sydney), and the Sydney Children's Hospital Network, by grants from the National Health and Medical Research (Program Grant APP1091261, Senior Research Fellowship APP1161216 to A.S., APP1144113 for J.M., and Principal Research Fellowship APP1119152 to M.K.), and by a Cancer Institute New South Wales Program grant (TPG2037 to M.K.). M.K and T.P.D. are supported by the Australian Research Council Centre of Excellence in Convergent Bio-Nano Science and Technology (CE140100036). Aspects of this work were funded through Cancer Australia/Kids Cancer Project (APP1184840, J.M., T.P.D., M.K.) and the Olivia Lambert Foundation (J.M.). The authors thank the Sydney Children's Tumor Bank Network (Children's Cancer Institute Tumor Bank) for providing samples and related clinical information for this study and the Children's Cancer Institute Animal Facility for providing support to this study. The authors would also like to acknowledge the Ramaciotti Center for Genomics, the Garvan Histopathology facility, and the Neuroblastoma Research Consortium (NRC) for sharing the miRNA and copy-number data. The graphical abstract was created with BioRender.com.

AUTHOR CONTRIBUTIONS

Conceptualization, A.S., J.F., and G.M.M.; investigation, H.H., J.Y., E.D., I.N., A.K., M.W., and S.A.; data curation, H.H., N.D., I.N., K.S., P.M., and K.d.P.; formal analysis, N.D., P.M., H.H., I.N., K.S., and C.E.C.; writing – original draft, H.H.; writing – review & editing, I.N., J.Y., J.M., G.M.M., K.J.S., J.F., S.A., and A.S.; resources, J.F., J.M., T.P.D., and M.K.; funding acquisition, A.S., J.F., and G.M.M.; supervision, A.S.

DECLARATION OF INTERESTS

The authors declare no competing interests.

REFERENCES

1. Matthay, K.K., Maris, J.M., Schleiermacher, G., Nakagawara, A., Mackall, C.L., Diller, L., and Weiss, W.A. (2016). Neuroblastoma. Nat. Rev. Dis. Prim. *2*, 16078. https://doi.org/10.1038/nrdp.2016.78.

2. Durinck, K., and Speleman, F. (2018). Epigenetic regulation of neuroblastoma development. Cell Tissue Res. *372*, 309–324. https://doi.org/10.1007/s00441-017-2773-y.

3. Brodeur, G.M., Seeger, R.C., Schwab, M., Varmus, H.E., and Bishop, J.M. (1984). Amplification of N-myc in untreated human neuroblastomas correlates with advanced disease stage. Science (New York, N.Y.) *224*, 1121–1124. https://doi.org/10.1126/science.6719137.

4. Seeger, R.C., Brodeur, G.M., Sather, H., Dalton, A., Siegel, S.E., Wong, K.Y., and Hammond, D. (1985). Association of multiple copies of the N-myc oncogene with rapid progression of neuroblastomas. N. Engl. J. Med. *313*, 1111–1116. https://doi.org/10.1056/nejm198510313131802.

5. Applebaum, M.A., Vaksman, Z., Lee, S.M., Hungate, E.A., Henderson, T.O., London, W.B., Pinto, N., Volchenboum, S.L., Park, J.R., Naranjo, A., et al. (2017). Neuroblastoma survivors are at increased risk for second malignancies: a report from the International Neuroblastoma Risk Group Project. Eur. J. Cancer *72*, 177–185. https://doi.org/10.1016/j.ejca.2016.11.022.

6. Cohen, L.E., Gordon, J.H., Popovsky, E.Y., Gunawardene, S., Duffey-Lind, E., Lehmann, L.E., and Diller, L.R. (2014). Late effects in children treated with intensive multimodal therapy for high-risk neuroblastoma: high incidence of endocrine and growth problems. Bone Marrow Transplant. *49*, 502–508. https://doi.org/10.1038/bmt.2013.218.

7. Zheng, D.J., Krull, K.R., Chen, Y., Diller, L., Yasui, Y., Leisenring, W., Brouwers, P., Howell, R., Lai, J.S., Balsamo, L., et al. (2018). Long-term psychological and educational outcomes for survivors of neuroblastoma: a report from the Childhood Cancer Survivor Study. Cancer *124*, 3220–3230. https://doi.org/10.1002/cncr.31379.

8. Smith, V., and Foster, J. (2018). High-risk neuroblastoma treatment review. Children (Basel) *5*, 114. https://doi.org/10.3390/children5090114.

9. Trahair, T.N., Vowels, M.R., Johnston, K., Cohn, R.J., Russell, S.J., Neville, K.A., Carroll, S., and Marshall, G.M. (2007). Long-term outcomes in children with high-risk neuroblastoma treated with autologous stem cell transplantation. Bone Marrow Transplant. *40*, 741–746. https://doi.org/10.1038/sj.bmt.1705809.

10. He, L., and Hannon, G.J. (2004). MicroRNAs: small RNAs with a big role in gene regulation. Nat. Rev. Genet. *5*, 522–531. https://doi.org/10.1038/nrg1379.

11. Gurtan, A.M., and Sharp, P.A. (2013). The role of miRNAs in regulating gene expression networks. J. Mol. Biol. *425*, 3582–3600. https://doi.org/10.1016/j.jmb.2013.03.007.

12. Gebert, L.F.R., and MacRae, I.J. (2019). Regulation of microRNA function in animals. Nat. Rev. Mol. Cell Biol. *20*, 21–37. https://doi.org/10.1038/s41580-018-0045-7.

13. Alberti, C., and Cochella, L. (2017). A framework for understanding the roles of miRNAs in animal development. Development *144*, 2548. https://doi.org/10.1242/dev.146613.

14. Rupaimoole, R., and Slack, F.J. (2017). MicroRNA therapeutics: towards a new era for the management of cancer and other diseases. Nat. Rev. Drug Discov. *16*, 203–222. https://doi.org/10.1038/nrd.2016.246.

15. Lu, J., Getz, G., Miska, E.A., Alvarez-Saavedra, E., Lamb, J., Peck, D., Sweet-Cordero, A., Ebert, B.L., Mak, R.H., Ferrando, A.A., et al. (2005). MicroRNA expression profiles classify human cancers. Nature *435*, 834–838. https://doi.org/10.1038/nature03702.

16. Welch, C., Chen, Y., and Stallings, R.L. (2007). MicroRNA-34a functions as a potential tumor suppressor by inducing apoptosis in neuroblastoma cells. Oncogene *26*, 5017–5022. https://doi.org/10.1038/sj.onc.1210293.

17. Swarbrick, A., Woods, S.L., Shaw, A., Balakrishnan, A., Phua, Y., Nguyen, A., Chanthery, Y., Lim, L., Ashton, L.J., Judson, R.L., et al. (2010). miR-380-5p represses p53 to control cellular survival and is associated with poor outcome in MYCN-amplified neuroblastoma. Nat. Med. *16*, 1134–1140. https://doi.org/10.1038/nm.2227.

18. Mestdagh, P., Boström, A.-K., Impens, F., Fredlund, E., Van Peer, G., De Antonellis, P., von Stedingk, K., Ghesquière, B., Schulte, S., Dews, M., et al. (2010). The miR-17-92 microRNA cluster regulates multiple components of the TGF-β pathway in neuroblastoma. Mol. Cell *40*, 762–773. https://doi.org/10.1016/j.molcel.2010.11.038.

19. Molenaar, J.J., Domingo-Fernández, R., Ebus, M.E., Lindner, S., Koster, J., Drabek, K., Mestdagh, P., van Sluis, P., Valentijn, L.J., van Nes, J., et al. (2012). LIN28B induces neuroblastoma and enhances MYCN levels via let-7 suppression. Nat. Genet. *44*, 1199–1206. https://doi.org/10.1038/ng.2436.

20. Ooi, C.Y., Carter, D.R., Liu, B., Mayoh, C., Beckers, A., Lalwani, A., Nagy, Z., De Brouwer, S., Decaesteker, B., Hung, T.T., et al. (2018). Network modeling of microRNA-mRNA interactions in neuroblastoma tumorigenesis identifies miR-204 as a direct inhibitor of MYCN. Cancer Res. *78*, 3122–3134. https://doi.org/10.1158/0008-5472.can-17-3034.

21. Nikolic, I., Elsworth, B., Dodson, E., Wu, S.Z., Gould, C.M., Mestdagh, P., Marshall, G.M.,, Horvath, L.G., Simpson, K.J., and Swarbrick, A. (2017). Discovering cancer

vulnerabilities using high-throughput micro-RNA screening. Nucleic Acids Res. *45*, 12657–12670. https://doi.org/10.1093/nar/gkx1072.

22. He, L., He, X., Lim, L.P., de Stanchina, E., Xuan, Z., Liang, Y., Xue, W., Zender, L., Magnus, J., Ridzon, D., et al. (2007). A microRNA component of the p53 tumour suppressor network. Nature *447*, 1130–1134. https://doi.org/10.1038/nature05939.

23. Cole, K.A., Attiyeh, E.F., Mosse, Y.P., Laquaglia, M.J., Diskin, S.J., Brodeur, G.M., and Maris, J.M. (2008). A functional screen identifies miR-34a as a candidate neuroblastoma tumor suppressor gene. Mol. Cancer Res. *6*, 735–742. https://doi.org/10.1158/1541-7786.Mcr-07-2102.

24. Eulalio, A., Mano, M., Ferro, M.D., Zentilin, L., Sinagra, G., Zacchigna, S., and Giacca, M. (2012). Functional screening identifies miRNAs inducing cardiac regeneration. Nature *492*, 376–381. https://doi.org/10.1038/nature11739.

25. Roush, S., and Slack, F.J. (2008). The let-7 family of microRNAs. Trends Cell Biol. *18*, 505–516. https://doi.org/10.1016/j.tcb.2008.07.007.

26. Wang, J.K., Wang, Z., and Li, G. (2019). MicroRNA-125 in immunity and cancer. Cancer Lett. *454*, 134–145. https://doi.org/10.1016/j.canlet.2019.04.015.

27. Mora, J., Cheung, N.K., Chen, L., Qin, J., and Gerald, W. (2001). Loss of heterozygosity at 19q13.3 is associated with locally aggressive neuroblastoma. Clin. Cancer Res. *7*, 1358–1361.

28. Uryu, K., Nishimura, R., Kataoka, K., Sato, Y., Nakazawa, A., Suzuki, H., Yoshida, K., Seki, M., Hiwatari, M., Isobe, T., et al. (2017). Identification of the genetic and clinical characteristics of neuroblastomas using genome-wide analysis. Oncotarget *8*, 107513–107529. https://doi.org/10.18632/oncotarget.22495.

29. Hoshi, M., Otagiri, N., Shiwaku, H.O., Asakawa, S., Shimizu, N., Kaneko, Y., Ohi, R., Hayashi, Y., and Horii, A. (2000). Detailed deletion mapping of chromosome band 14q32 in human neuroblastoma defines a 1.1-Mb region of common allelic loss. Br. J. Cancer *82*, 1801–1807. https://doi.org/10.1054/bjoc.2000.1108.

30. Thompson, P.M., Seifried, B.A., Kyemba, S.K., Jensen, S.J., Guo, C., Maris, J.M., Brodeur, G.M., Stram, D.O., Seeger, R.C., Gerbing, R., et al. (2001). Loss of heterozygosity for chromosome 14q in neuroblastoma. Med. Pediatr. Oncol. *36*, 28–31. https://doi.org/10.1002/1096-911x(20010101)36:1<28::Aid-mpo1008>3.0.Co;2-0.

31. Depuydt, P., Boeva, V., Hocking, T.D., Cannoodt, R., Ambros, I.M., Ambros, P.F., Asgharzadeh, S., Attiyeh, E.F., Combaret, V., Defferrari, R., et al. (2018). Genomic amplifications and distal 6q loss: novel markers for poor survival in high-risk neuroblastoma patients. J. Natl. Cancer Inst. *110*, 1084–1093. https://doi.org/10.1093/jnci/djy022.

32. Harenza, J.L., Diamond, M.A., Adams, R.N., Song, M.M., Davidson, H.L., Hart, L.S., Dent, M.H., Fortina, P., Reynolds, C.P., and Maris, J.M. (2017). Transcriptomic profiling of 39 commonly-used neuroblastoma cell lines. Sci. Data *4*, 170033. https://doi.org/10.1038/sdata.2017.33.

33. Ling, Y.H., el-Naggar, A.K., Priebe, W., and Perez-Soler, R. (1996). Cell cycle-dependent cytotoxicity, G2/M phase arrest, and disruption of p34cdc2/cyclin B1 activity induced by doxorubicin in synchronized P388 cells. Mol. Pharmacol. *49*, 832–841.

34. van Groningen, T., Akogul, N., Westerhout, E.M., Chan, A., Hasselt, N.E., Zwijnenburg, D.A., Broekmans, M., Stroeken, P., Haneveld, F., Hooijer, G.K.J., et al. (2019). A NOTCH feed-forward loop drives reprogramming from adrenergic to mesenchymal state in neuroblastoma. Nat. Commun. *10*, 1530. https://doi.org/10.1038/s41467-019-09470-w.

35. Kostopoulou, O.N., Holzhauser, S., Lange, B.K.A., Ohmayer, A., Andonova, T., Bersani, C., Wickström, M., and Dalianis, T. (2019). Analyses of FGFR3 and PIK3CA mutations in neuroblastomas and the effects of the corresponding inhibitors on neuroblastoma cell lines. Int. J. Oncol. *55*, 1372–1384. https://doi.org/10.3892/ijo.2019.4896.

36. Ma, S., Jia, R., Li, D., and Shen, B. (2015). Targeting cellular metabolism chemosensitizes the doxorubicin-resistant human breast adenocarcinoma cells. Biomed. Res. Int. *2015*, 453986. https://doi.org/10.1155/2015/453986.

37. Sun, D., Lee, Y.S., Malhotra, A., Kim, H.K., Matecic, M., Evans, C., Jensen, R.V., Moskaluk, C.A., and Dutta, A. (2011). miR-99 family of MicroRNAs suppresses the expression of prostate-specific antigen and prostate cancer cell proliferation. Cancer Res. *71*, 1313–1324. https://doi.org/10.1158/0008-5472.can-10-1031.

38. Wei, F., Liu, Y., Guo, Y., Xiang, A., Wang, G., Xue, X., and Lu, Z. (2013). miR-99b-targeted mTOR induction contributes to irradiation resistance in pancreatic cancer. Mol. Cancer *12*, 81. https://doi.org/10.1186/1476-4598-12-81.

39. Teo, J., McCarroll, J.A., Boyer, C., Youkhana, J., Sagnella, S.M., Duong, H.T., Liu, J., Sharbeen, G., Goldstein, D., Davis, T.P., et al. (2016). A rationally optimized nanoparticle system for the delivery of RNA interference therapeutics into pancreatic tumors in vivo. Biomacromolecules *17*, 2337–2351. https://doi.org/10.1021/acs.biomac.6b00185.

40. Reid, G., Pel, M.E., Kirschner, M.B., Cheng, Y.Y., Mugridge, N., Weiss, J., Williams, M., Wright, C., Edelman, J.J., Vallely, M.P., et al. (2013). Restoring expression of miR-16: a novel approach to therapy for malignant pleural mesothelioma. Ann. Oncol.: Off. J. Eur. Soc. Med. Oncol. *24*, 3128–3135. https://doi.org/10.1093/annonc/mdt412.

41. Boeva, V., Louis-Brennetot, C., Peltier, A., Durand, S., Pierre-Eugene, C., Raynal, V., Etchevers, H.C., Thomas, S., Lermine, A., Daudigeos-Dubus, E., et al. (2017). Heterogeneity of neuroblastoma cell identity defined by transcriptional circuitries. Nat. Genet. *49*, 1408–1413. https://doi.org/10.1038/ng.3921.

42. van Groningen, T., Koster, J., Valentijn, L.J., Zwijnenburg, D.A., Akogul, N., Hasselt, N.E., Broekmans, M., Haneveld, F., Nowakowska, N.E., Bras, J., et al. (2017). Neuroblastoma is composed of two super-enhancer-associated differentiation states. Nat. Genet. *49*, 1261–1266. https://doi.org/10.1038/ng.3899.

43. Durbin, A.D., Zimmerman, M.W., Dharia, N.V., Abraham, B.J., Iniguez, A.B., Weichert-Leahey, N., He, S., Krill-Burger, J.M., Root, D.E., Vazquez, F., et al. (2018). Selective gene dependencies in MYCN-amplified neuroblastoma include the core transcriptional regulatory circuitry. Nat. Genet. *50*, 1240–1246. https://doi.org/10.1038/s41588-018-0191-z.

44. Meyers, R.M., Bryan, J.G., McFarland, J.M., Weir, B.A., Sizemore, A.E., Xu, H., Dharia, N.V., Montgomery, P.G., Cowley, G.S., Pantel, S., et al. (2017). Computational correction of copy number effect improves specificity of CRISPR-Cas9 essentiality screens in cancer cells. Nat. Genet. *49*, 1779–1784. https://doi.org/10.1038/ng.3984.

45. Broad, D. (2020). DepMap 20Q4 Public. figshare. Dataset. https://doi.org/10.6084/m9.figshare.13237076.v2.

46. Betel, D., Koppal, A., Agius, P., Sander, C., and Leslie, C. (2010). Comprehensive modeling of microRNA targets predicts functional non-conserved and non-canonical sites. Genome Biol. *11*, R90. https://doi.org/10.1186/gb-2010-11-8-r90.

47. Paraskevopoulou, M.D., Georgakilas, G., Kostoulas, N., Vlachos, I.S., Vergoulis, T., Reczko, M., Filippidis, C., Dalamagas, T., and Hatzigeorgiou, A.G. (2013). DIANA-microT web server v5.0: service integration into miRNA functional analysis workflows. Nucleic Acids Res. *41*, W169–W173. https://doi.org/10.1093/nar/gkt393.

48. Bachetti, T., Di Zanni, E., Ravazzolo, R., and Ceccherini, I. (2015). miR-204 mediates post-transcriptional down-regulation of PHOX2B gene expression in neuroblastoma cells. Biochim. Biophys. Acta (BBA) - Gene Regul. Mech. *1849*, 1057–1065. https://doi.org/10.1016/j.bbagrm.2015.06.008.

49. Wang, Z., Zhao, Z., Yang, Y., Luo, M., Zhang, M., Wang, X., Liu, L., Hou, N., Guo, Q., Song, T., et al. (2018). MiR-99b-5p and miR-203a-3p function as tumor suppressors by targeting IGF-1R in gastric cancer. Sci. Rep. *8*, 10119. https://doi.org/10.1038/s41598-018-27583-y.

50. Kang, J., Lee, S.Y., Lee, S.Y., Kim, Y.J., Park, J.Y., Kwon, S.J., Na, M.J., Lee, E.J., Jeon, H.S., and Son, J.W. (2012). microRNA-99b acts as a tumor suppressor in non-small cell lung cancer by directly targeting fibroblast growth factor receptor 3. Exp. Ther. Med. *3*, 149–153. https://doi.org/10.3892/etm.2011.366.

51. Liu, R., Chen, Y., Shou, T., Hu, J., and Qing, C. (2019). miRNA-99b-5p targets FZD8 to inhibit non-small cell lung cancer proliferation, migration and invasion. Onco Targets Ther. *12*, 2615–2621. https://doi.org/10.2147/ott.S199196.

52. Li, W., Chang, J., Wang, S., Liu, X., Peng, J., Huang, D., Sun, M., Chen, Z., Zhang, W., Guo, W., and Li, J. (2015). miRNA-99b-5p suppresses liver metastasis of colorectal cancer by down-regulating mTOR. Oncotarget *6*, 24448–24462. https://doi.org/10.18632/oncotarget.4423.

53. Wang, Z.Q., Zhang, M.Y., Deng, M.L., Weng, N.Q., Wang, H.Y., and Wu, S.X. (2017). Low serum level of miR-485-3p predicts poor survival in patients with glioblastoma. PLoS One *12*, e0184969. https://doi.org/10.1371/journal.pone.0184969.

54. Mao, K., Lei, D., Zhang, H., and You, C. (2017). MicroRNA-485 inhibits malignant biological behaviour of glioblastoma cells by directly targeting PAK4. Int. J. Oncol. *51*, 1521–1532. https://doi.org/10.3892/ijo.2017.4122.

55. Lou, C., Xiao, M., Cheng, S., Lu, X., Jia, S., Ren, Y., and Li, Z. (2016). MiR-485-3p and miR-485-5p suppress breast cancer cell metastasis by inhibiting PGC-1alpha expression. Cell Death Dis. *7*, e2159. https://doi.org/10.1038/cddis.2016.27.

56. Chen, C.F., He, X., Arslan, A.D., Mo, Y.Y., Reinhold, W.C., Pommier, Y., and Beck, W.T. (2011). Novel regulation of nuclear factor-YB by miR-485-3p affects the expression of DNA topoisomerase IIalpha and drug responsiveness. Mol. Pharmacol. *79*, 735–741. https://doi.org/10.1124/mol.110.069633.

57. Cai, Z., Zheng, F., Ding, Y., Zhan, Y., Gong, R., Li, J., Aschner, M., Zhang, Q., Wu, S., and Li, H. (2019). Nrf2-regulated miR-380-3p blocks the translation of Sp3 protein and its mediation of paraquat-induced toxicity in mouse neuroblastoma N2a cells. Toxicol. Sci. *171*, 515–529. https://doi.org/10.1093/toxsci/kfz162.

58. Zhang, Z., Pi, J., Zou, D., Wang, X., Xu, J., Yu, S., Zhang, T., Li, F., Zhang, X., Zhao, H., et al. (2019). microRNA arm-imbalance in part from complementary targets mediated decay promotes gastric cancer progression. Nat. Commun. *10*, 4397. https://doi.org/10.1038/s41467-019-12292-5.

59. Wesche, J., Haglund, K., and Haugsten, Ellen M. (2011). Fibroblast growth factors and their receptors in cancer. Biochem. J. *437*, 199–213. https://doi.org/10.1042/BJ20101603.

60. Gartlgruber, M., Sharma, A.K., Quintero, A., Dreidax, D., Jansky, S., Park, Y.-G., Kreth, S., Meder, J., Doncevic, D., Saary, P., and Toprak, U.H. (2021). Super enhancers define regulatory subtypes and cell identity in neuroblastoma. Nat. Cancer *2*, 114–128. https://doi.org/10.1038/s43018-020-00145-w.

61. Schnepp, R.W., Khurana, P., Attiyeh, E.F., Raman, P., Chodosh, S.E., Oldridge, D.A., Gagliardi, M.E., Conkrite, K.L., Asgharzadeh, S., Seeger, R.C., et al. (2015). A LIN28B-RAN-AURKA signaling network promotes neuroblastoma tumorigenesis. Cancer Cell *28*, 599–609. https://doi.org/10.1016/j.ccell.2015.09.012.

62. Vishnubalaji, R., Elango, R., Al-Toub, M., Manikandan, M., Al-Rikabi, A., Harkness, L., Ditzel, N., Atteya, M., Hamam, R., Alfayez, M., et al. (2019). Neoplastic transformation of human mesenchymal stromal cells mediated via LIN28B. Sci. Rep. *9*, 8101. https://doi.org/10.1038/s41598-019-44536-1.

63. Tao, T., Shi, H., Mariani, L., Abraham, B.J., Durbin, A.D., Zimmerman, M.W., Powers, J.T., Missios, P., Ross, K.N., Perez-Atayde, A.R., et al. (2020). LIN28B regulates transcription and potentiates MYCN-induced neuroblastoma through binding to ZNF143 at target gene promotors. Proc. Natl. Acad. Sci. *117*, 201922692. https://doi.org/10.1073/pnas.1922692117.

64. Martirosyan, A., Clendening, J.W., Goard, C.A., and Penn, L.Z. (2010). Lovastatin induces apoptosis of ovarian cancer cells and synergizes with doxorubicin: potential therapeutic relevance. BMC Cancer *10*, 103. https://doi.org/10.1186/1471-2407-10-103.

65. Kozar, K., Kaminski, R., Legat, M., Kopec, M., Nowis, D., Skierski, J.S., Koronkiewicz, M., Jakóbisiak, M., and Golab, J. (2004). Cerivastatin demonstrates enhanced antitumor activity against human breast cancer cell lines when used in combination with doxorubicin or cisplatin. Int. J. Oncol. *24*, 1149–1157.

66. Fromigué, O., Hamidouche, Z., and Marie, P.J. (2008). Statin-induced inhibition of 3-hydroxy-3-methyl glutaryl coenzyme a reductase sensitizes human osteosarcoma cells to anticancer drugs. J. Pharmacol. Exp. Ther. *325*, 595–600. https://doi.org/10.1124/jpet.108.136127.

67. Babichev, Y., Kabaroff, L., Datti, A., Uehling, D., Isaac, M., Al-Awar, R., Prakesch, M., Sun, R.X., Boutros, P.C., Venier, R., et al. (2016). PI3K/AKT/mTOR inhibition in combination with doxorubicin is an effective therapy for leiomyosarcoma. J. Transl. Med. *14*, 67. https://doi.org/10.1186/s12967-016-0814-z.

68. Li, J., Liu, W., Hao, H., Wang, Q., and Xue, L. (2019). Rapamycin enhanced the antitumor effects of doxorubicin in myelogenous leukemia K562 cells by downregulating the mTOR/p70S6K pathway. Oncol. Lett. *18*, 2694–2703. https://doi.org/10.3892/ol.2019.10589.

69. van Zandwijk, N., Pavlakis, N., Kao, S.C., Linton, A., Boyer, M.J., Clarke, S., Huynh, Y., Chrzanowska, A., Fulham, M.J., Bailey, D.L., et al. (2017). Safety and activity of microRNA-loaded minicells in patients with recurrent malignant pleural mesothelioma: a first-in-man, phase 1, open-label, dose-escalation study. Lancet Oncol. *18*, 1386–1396. https://doi.org/10.1016/s1470-2045(17)30621-6.

70. De Preter, K., Mestdagh, P., Vermeulen, J., Zeka, F., Naranjo, A., Bray, I., Castel, V., Chen, C., Drozynska, E., Eggert, A., et al. (2011). miRNA expression profiling enables risk stratification in archived and fresh neuroblastoma tumor samples. Clin. Cancer Res. *17*, 7684. https://doi.org/10.1158/1078-0432.CCR-11-0610.

71. Rajbhandari, P., Lopez, G., Capdevila, C., Salvatori, B., Yu, J., Rodriguez-Barrueco, R., Martinez, D., Yarmarkovich, M., Weichert-Leahey, N., Abraham, B.J., et al. (2018). Cross-cohort analysis identifies a TEAD4–MYCN positive feedback loop as the core regulatory element of high-risk neuroblastoma. Cancer Discov. *8*, 582. https://doi.org/10.1158/2159-8290.CD-16-0861.

72. Andrews, S. (2010). FastQC: a quality control tool for high throughput sequence data. bioinformatics.babraham.ac.uk/projects/fastqc.

73. Dobin, A., Davis, C.A., Schlesinger, F., Drenkow, J., Zaleski, C., Jha, S., Batut, P., Chaisson, M., and Gingeras, T.R. (2013). STAR: ultrafast universal RNA-seq aligner. Bioinformatics (Oxford, England) *29*, 15–21. https://doi.org/10.1093/bioinformatics/bts635.

74. Li, B., and Dewey, C.N. (2011). RSEM: accurate transcript quantification from RNA-Seq data with or without a reference genome. BMC Bioinf. *12*, 323. https://doi.org/10.1186/1471-2105-12-323.

75. Ritchie, M.E., Phipson, B., Wu, D., Hu, Y., Law, C.W., Shi, W., and Smyth, G.K. (2015). Limma powers differential expression analyses for RNA-sequencing and microarray studies. Nucleic Acids Res. *43*, e47. https://doi.org/10.1093/nar/gkv007.

76. Liao, Y., Wang, J., Jaehnig, E.J., Shi, Z., and Zhang, B. (2019). WebGestalt 2019: gene set analysis toolkit with revamped UIs and APIs. Nucleic Acids Res. *47*, W199–W205. https://doi.org/10.1093/nar/gkz401.